Activation And In Situ Ethylene Polymerization On Silica-Supported Ziegler-Natta Catalysts

ARTICLE *in* ACS CATALYSIS · AUGUST 2015

Impact Factor: 9.31 · DOI: 10.1021/acscatal.5b01108

6 AUTHORS, INCLUDING:

Kalaivani Seenivasan
Stella Maris College
12 PUBLICATIONS **133** CITATIONS
SEE PROFILE

Anna Sommazzi
Research Center for Non Conventional Energy
40 PUBLICATIONS **594** CITATIONS
SEE PROFILE

Carlo Lamberti
Università degli Studi di Torino
382 PUBLICATIONS **13,130** CITATIONS
SEE PROFILE

ACS Catalysis

Research Article

pubs.acs.org/acscatalysis

Activation and In Situ Ethylene Polymerization on Silica-Supported Ziegler–Natta Catalysts

Elena Groppo,*[,†] Kalaivani Seenivasan,[†] Erik Gallo,[†,‡] Anna Sommazzi,[§] Carlo Lamberti,[∥,⊥] and Silvia Bordiga[†]

[†]Department of Chemistry, INSTM and NIS Centre, University of Torino, Via Quarello 15, 10135 Torino, Italy

[‡]European Synchrotron Radiation Facility, 6 Rue Jules Horowitz, 38043 Grenoble, France

[§]Versalis – Novara Research Center, Istituto Eni Donegani, Via Fauser, 4, 28100 Novara, Italy

[∥]Department of Chemistry, INSTM and CrisDi Centre, University of Torino, Via Giuria 7, 10125 Torino, Italy

[⊥]Southern Federal University, Zorge Street 5, 344090 Rostov-on-Don, Russia

ABSTRACT: The structural, vibrational, and electronic properties of silica-supported Ziegler–Natta catalysts industrially relevant for polyethylene production were investigated in detail by means of a multitechnical approach at each step of catalyst preparation, including precatalyst activation. In the precatalyst, the $TiCl_x$ phase is grafted mainly to the silica surface and almost independent of the supported $MgCl_x$ phase. However, the subsequent activation by means of an aluminum–alkyl compound causes important changes to both the supported $MgCl_x$ phase and the $TiCl_x$ phase. The resulting catalyst is entirely reconstructed so that most of the titanium sites are detached from the silica surface and in interaction with a highly dispersed $MgCl_2$ phase, thus mimicking the most famous and highly investigated Ziegler–Natta catalysts (not silica-supported). For the first time, the catalyst performances were monitored by means of in situ FT-IR spectroscopy in transmission mode, simulating industrially significant polymerization conditions (i.e., ethylene is fed onto the catalyst in the presence of the activator and the solvent). These results demonstrate that it is now possible to achieve a complete description at a molecular level of all the constituents of Ziegler–Natta catalysts and at each step of the catalyst preparation.

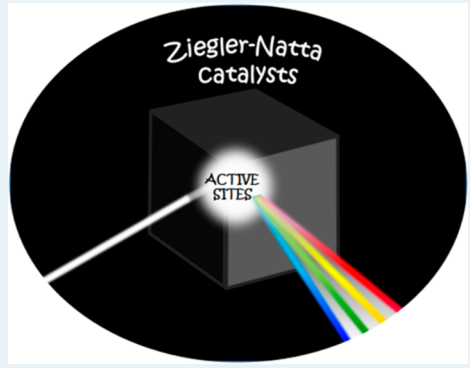

KEYWORDS: *Ziegler–Natta catalysts, polyethylene, polymerization, in situ spectroscopic techniques, silica*

1. INTRODUCTION

Heterogeneous Ziegler–Natta catalysts for production of polyolefins are among the most employed and versatile catalysts in the chemical industry and probably those having the largest impact not only in science but also in everyday life. The extraordinarily large number of polymer architectures today available and the remarkable rapid progress in polyolefin technology are closely associated with the catalyst's development and innovation in process technology. Since their discovery in 1960s, heterogeneous Ziegler–Natta catalysts have progressed enormously, making it possible to produce advanced polyolefin materials having tailored properties. Today, Ziegler–Natta catalysis allows a precision synthesis of polyolefins based on the exact assembly of the olefin monomers at the nanoscale through the intervention of the active catalytic sites.[1−3]

Most of the breakthrough in this field was the result of a trial-and-error approach, commonly adopted not only in the chemical industries involved in polyolefin production but also in academic laboratories. The opposite method to improve the catalyst's performances, that is, a full elucidation of the catalyst's structure by means of combined spectroscopic and structural experimental methods, is much less widespread.[4] In situ investigation of heterogeneous Ziegler–Natta catalysts is hampered by two main problems: (i) the active species are only a few in number (whereas the majority are spectators), which altogether determine the behavior of the catalytic system, and (ii) the ease of contamination, which implies that comparing or combining data obtained in different laboratories is risky.[5] For these reasons, so far, most of the experimental investigations on heterogeneous Ziegler–Natta systems have been focused on the precatalyst only, that is, the system before interaction with the activator, usually an aluminum–alkyl compound. Precatalysts are simpler in chemical composition and much less sensitive to contamination. Although the properties of the precatalyst might have an influence on those of the catalyst, it was demonstrated that the activator causes a substantial transformation in the precatalyst involving all the components, not merely the active phase.[5−8] Therefore, elucidation of the catalyst structure requires the ability to investigate the system in the presence of the activator if not in

Received: May 27, 2015
Revised: August 12, 2015
Published: August 13, 2015

DOI: 10.1021/acscatal.5b01108
ACS Catal. 2015, 5, 5586−5595

the presence of both the activator and the olefin monomer, that is, under reaction conditions.

In situ and operando studies are nowadays common in catalysis and have provided substantial progress in the understanding of the catalyst's performance in many important catalytic processes.[9−19] The experimental tools have progressed enormously in recent years, allowing investigation of the catalysts in action, even under extreme conditions (high temperature, high pressure, etc.) and with increasing time and space resolution. Unfortunately, application of these methods to Ziegler−Natta catalysts is still in the early stages.[5] Among the few studies on Ziegler−Natta catalysts in action, we mention the in situ optical observation of growing polypropylene particles on heterogeneous Ziegler−Natta catalysts.[20,21] Although fascinating, these results give information on the kinetics of the polymerization only; they are not informative about the structure of the active sites on a molecular scale. A few efforts in this direction have been attempted by means of surface science methods applied to planar models of Ziegler−Natta catalysts. Thune and his group developed a smart experimental setup that allows monitoring of each step of catalyst preparation (including precatalyst activation) and olefin polymerization by means of in situ attenuated total reflection (ATR) IR spectroscopy.[22−25] Very recently, a detailed characterization of potential catalytically active sites in an activated $MgCl_2$-supported industrial Ziegler−Natta catalyst was also achieved by means of advanced EPR techniques[26] that, however, are completely silent toward all other catalysts' constituents. Hence, we could safely say that, despite these efforts, the structural and electronic properties of the titanium active sites and their relation to the catalytic body as a whole in heterogeneous Ziegler−Natta catalysts remain substantially a black box.

Recently, we have been involved in a systematic investigation of heterogeneous Ziegler−Natta catalysts based on titanium and magnesium chloride tetrahydrofuranates, which were patented in the early 1970s[27,28] and are facing a revival in the recent years because of the increasing attention of academic laboratories.[5,7,8,29−31] In our previous works, we have demonstrated the potential of a multitechnique approach in unraveling the nature of the active $TiCl_x$ phase in catalysts obtained by reacting together titanium and magnesium chloride tetrahydrofuranate precursors and the aluminum−alkyl activator.[7,8] The investigation is more complex when the $TiCl_x$ and $MgCl_x$ phases are simultaneously supported on dehydroxylated silica in the presence of tetrahydrofuran. This catalyst was developed in the 1980s by a group of scientists from Union Carbide Corporation to be used in the UNIPOL process to produce high-density polyethylene.[32−38]

The use of polymer-grade dehydroxylated silica as a support in polymerization catalysts is nowadays quite common because it provides a larger surface area along with good control of the polymer morphology.[38−42] Although silica is often described just as a template to produce polyethylene particles having the right particle size and particle size distribution suitable for gas-phase processes, it is now well documented that it also plays an active role in defining the properties of the catalyst as a whole.[5,43−46] The simpler SiO_2/Ti system (where Ti is $TiCl_4(thf)_2$ precursor, and thf is tetrahydrofuran) has been the subject of a previous investigation by means of X-ray powder diffraction (XRPD), FT-IR, UV−vis, X-ray absorption spectroscopy (XAS), and valence-to-core X-ray emission spectroscopy (vtc-XES) techniques.[47] We have demonstrated that the synergic combination of these techniques allows achieving a complete scenario on the properties of the supported titanium phase. Herein, we proceeded with the investigation by looking at the SiO_2/TiMg precatalyst (where Ti is the $TiCl_4(thf)_2$ precursor, and Mg is the $MgCl_2(thf)_{1.5}$ precursor) and at the catalyst originating after interaction with the aluminum−alkyl activator (TOAl is trioctylaluminum). The whole arsenal of characterization techniques cited above allowed us to obtain information on the role of the activator in constructing the catalytically active phase not only in terms of titanium sites but also considering the $MgCl_x$ phase as well as the thf donor and the silica support. Ultimately, we looked at the catalyst in action by means of in situ FT-IR spectroscopy, mimicking industrially significant ethylene polymerization conditions.

2. EXPERIMENTAL SECTION

2.1. Materials. Davison sylopol silica 955 grade (surface area = 276 m^2/g, pore volume = 1.76 mL/g, average pore diameter = 266 Å, average particle size = 31 μm) was used as the support after a pretreatment in air at 550 °C for 8 h, followed by a cooling step carried out in nitrogen atmosphere. $TiCl_4(thf)_2$ and $MgCl_2(thf)_{1.5}$ precursors were synthesized following a procedure reported elsewhere.[48] The silica-supported samples were prepared by following a procedure similar to that adopted in our previous work[47] and in agreement with that reported in the original patents.[32,33] Briefly, the two precursors were dissolved in dry tetrahydrofuran and impregnated on dehydroxylated SiO_2 under a controlled atmosphere, using a Schlenk technique, resulting in a titanium loading of 4 wt % and a magnesium loading of 1.6 wt %. The excess of the solvent was further removed by gently heating the sample to ∼60 °C. The resulting precatalyst will be called hereafter SiO_2/TiMg. Single-phase silica-supported samples having the same amount of titanium (or magnesium) were prepared following the same method; these samples will be referred in the following as SiO_2/Ti and SiO_2/Mg.

The catalyst was prepared from precatalyst (in the form of powder or pellet, depending on the measurement) upon impregnation with trioctylaluminum (TOAl, Aldrich, 25% diluted in heptane, Al/Ti ∼ 10:1), inside a N_2-filled glovebox. This preparation step was always accomplished immediately before the measurement to prevent catalyst deactivation. The thus-prepared catalyst (hereafter, SiO_2/TiMg/TOAl) was then transferred into the measurement cell. For in situ FT-IR measurements during polymerization, deuterated ethylene (equilibrium pressure $P_{C_2D_4}$ = 100 mbar) was directly dosed into the reaction cell after the evacuation of N_2. This procedure was found to be critical because removal of N_2 may also cause a partial removal of the heptane solvent, followed by a fast deactivation of the catalyst. For this reason, evacuation of N_2 was performed by keeping the catalyst cold by means of a liquid nitrogen cold point. Then the catalyst was allowed to warm to room temperature, followed by dosage of ethylene-*d* into the measurement cell.

Table 1 contains a summary of all the samples investigated in this work, of the short labels, and of the corresponding entries as adopted in the Figures.

2.2. Techniques. *XRPD.* X-ray powder diffraction patterns were collected with a PW3050/60 X'Pert PRO MPD diffractometer from PANalytical working in Debye−Scherrer geometry, using as source a Cu anode filtered by a Ni foil to

DOI: 10.1021/acscatal.5b01108
ACS Catal. 2015, 5, 5586−5595

Table 1. Summary of All the Samples Investigated in This Work

entry	short label	full name
0	Mg	$MgCl_2(thf)_{1.5}$
1	SiO_2/Mg	$SiO_2/MgCl_2(thf)_{1.5}$
1′	SiO_2/Ti	$SiO_2/TiCl_4(thf)_2$
2	SiO_2/TiMg	$SiO_2/TiCl_4(thf)_2/MgCl_2(thf)_{1.5}$
3	SiO_2/TiMg/TOAl	$SiO_2/TiCl_4(thf)_2/MgCl_2(thf)_{1.5}$ + TOAl
4	SiO_2/TiMg/TOAl + C_2D_4	$SiO_2/TiCl_4(thf)_2/MgCl_2(thf)_{1.5}$ + TOAl + C_2D_4

attenuate the Kβ line and focused by a PW3152/63 X-ray mirror (λ = 1.5409 Å). The samples were measured as powders inside a 0.8 mm boron silicate capillary sealed in inert atmosphere.

X-ray Absorption Spectroscopy (EXAFS and XANES). Ti K-edge EXAFS spectra were collected at the BM26A beamline (DUBBLE) at the European Synchrotron Radiation Facility (ESRF, Grenoble, France).[49] The white beam was monochromatized using a Si(111) double crystal; harmonic rejection was performed by using silicon mirrors. Because the Ti K-edge was the lowest energy feasible at DUBBLE and the samples investigated were quite inhomogeneous, it was mandatory to develop a full feedback strategy for keeping full beamline flux while keeping beam delivery at a fixed exit point. EXAFS scans at low energies bring out the worst of the monochromators alignment issues and exit beam swing. To this purpose, two feedback systems were implemented:[50] (i) a position feedback to keep the beam delivered at a single vertical position within a 2 μm window (it acts on the mirrors) within the whole EXAFS scan and (ii) a I_0 feedback to keep the I_0 optimal throughout the EXAFS scan (it acts on the second crystal of the monochromator).

Because of titanium dilution and the absorbing nature of the support, EXAFS spectra were collected in fluorescence mode, by means of a nine-element germanium monolithic detector. The intensity of the incident beam was monitored by an ionization chamber filled with 1.2 bar of 5% N_2/95% He mixture, resulting in a 10% efficiency in the middle of the EXAFS scan. All the samples were manipulated under a controlled atmosphere inside an argon-filled glovebox. The samples were measured in the form of self-standing pellets inside a homemade quartz cell equipped with two kapton windows. Argon was removed from the cell before the measurement, because it absorbs a high fraction of the incoming beam at the low energy of the Ti K-edge. For the catalyst in the presence of TOAl, care was taken to remove argon by keeping the sample cold to avoid removal of TOAl or heptane (or both) and consequent deactivation of the catalyst.

The XANES part of the spectra was acquired with an energy step of 0.4 eV and an integration time of 2s/point. The EXAFS part of the spectra was collected up to 12 Å^{-1} with a variable sampling step in energy, resulting in a constant sampling step in k space of Δk = 0.05 Å^{-1} and an integration time that linearly increases as a function of k from 5 to 20 s/point to account for the low signal-to-noise ratio at high k values. For each sample, at least four equivalent EXAFS spectra were acquired and averaged before the data analysis. The extraction of the $\chi(k)$ functions was performed using the Athena program.[51] Once extracted, the k^3-weighted $\chi(k)$ functions were Fourier transformed in the Δk = 2.0−10.0 Å^{-1} range. This Δk interval has been selected in a conservative way, that is, to avoid the introduction of false signals in the FT. The fits were performed in R space (in the ΔR = 1.0−3.0 Å range, resulting in a maximum number of independent parameters $2\Delta k\Delta R/\pi$ larger than 10), using the Arthemis program.[51] Phase and amplitudes were calculated by FEFF6.0 code.[52]

X-ray Emission Spectroscopy. XES experiments were performed at beamline ID26 of the European Synchrotron Radiation Facility. The incident energy ($\hbar\Omega$) was selected by means of a pair of cryogenically cooled Si(311) single crystals (higher harmonics were suppressed by three Si mirrors operating in total reflection). The fluorescence photon energy ($\hbar\omega$) was selected using an emission spectrometer working in vertical Rowland geometry employing five Ge(331) spherically bent analyzer crystals of radius 1000 mm covering 70−110° in the horizontal scattering plane. The emitted photons were detected using an avalanche photodiode. The total energy bandwidth was 0.9 eV (as determined from the full width at half-maximum of the elastically scattered peak). The sample-to-crystal analyzer-to-photodiode path undergone by the Ti fluorescence photons occurs inside a slightly overpressured He bag, limiting the X-ray absorption. The samples were found to suffer from radiation damage on a fast time scale (about 10 s) due to the high photon flux adopted during vtc-XES measurements (more than 10^{12} photons per second). To circumvent this problem, each point of the vtc-XES spectrum was collected on a different sample spot irradiated for 2 s, and the intensity was normalized to the total fluorescence yield signal, integrated over the Ti Kα and Kβ lines recorded with a solid-state detector. The micrometric size of the beam and the large size of the sample (4 cm^2) allowed us to have sufficient fresh points on the sample to collect a full vtc-XES spectrum. As for XAS, the samples were measured in the form of self-supporting pellets prepared inside a glovebox and placed inside a cell with kapton windows. Also in this case, the cell was outgassed before measurements to remove argon, which absorbs most of the beam at this low energy. The background of the vtc-XES spectra, because of the K$\beta_{1,3}$ peak tail, was subtracted according to the procedure discussed in refs 53 and 54. Preliminary DFT calculations were performed within the one electron approximation using the ORCA 2008 code.[55]

Diffuse Reflectance UV−vis Spectroscopy (DR UV−vis). UV−vis−NIR spectra were collected in diffuse reflectance mode on a Cary5000 Varian spectrophotometer. All the samples were measured in the powdered form inside a cell having an optical window (Suprasil quartz) and allowing performance measurements under a controlled atmosphere.

IR Spectroscopy (Mid-IR and Far-IR). FT-IR spectra in the mid-IR region were acquired in transmission mode on a Bruker Vertex70 spectrophotometer equipped with a MCT detector at a resolution of 2 cm^{-1}. The samples were measured in the form of self-supporting pellets inside a quartz cell equipped with KBr windows under a controlled atmosphere. Far-IR spectra were collected at a resolution of 4 cm^{-1} with the same instrument after changing the optics (Si beam splitter) and the detector (far-IR DTGS). The samples were mixed with paraffin (which is perfectly transparent in the far-IR region) inside the glovebox and measured in the form of pellets. Paraffin protects the samples from air contamination at least for the time necessary to perform the measurement (a few minutes).

3. RESULTS AND DISCUSSION

3.1. From the Precatalyst to the Catalyst. *Identification of the Crystalline Phases.* The XRPD patterns of the SiO_2/

DOI: 10.1021/acscatal.5b01108
ACS Catal. 2015, 5, 5586−5595

TiMg precatalyst and of the catalyst are show in Figure 1, together with those of the magnesium chloride tetrahydrofura-

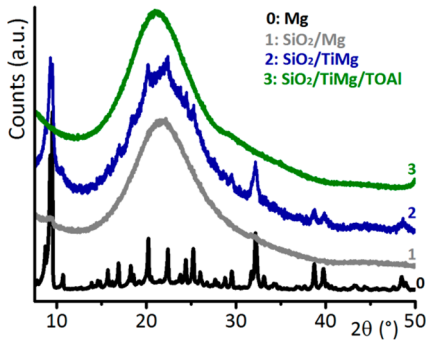

Figure 1. XRPD patterns (λ = 1.5409 Å) of magnesium chloride tetrahydrofuranates precursor (curve 0), SiO_2/Mg single-phase sample (curve 1), SiO_2/TiMg precatalyst (curve 2), and SiO_2/TiMg/TOAl catalyst (curve 3). The patterns have been vertically translated for clarity.

nate precursor and SiO_2/Mg. When the titanium and magnesium chloride tetrahydrofuranate precursors are simultaneously present on silica (curve 2), well-defined diffraction peaks are observed in the XRPD pattern, overlapped at the broad peak as a result of amorphous silica (2θ = 22°). The sharp peaks are characteristic of the crystalline magnesium precursor (curve 0).[7] It is important to notice that when the two titanium and magnesium chloride tetrahydrofuranate precursors are reacted together in thf solution in the absence of silica, a microcrystalline Ti−Mg ionic complex is formed, which is characterized by a peculiar XRPD pattern.[7,28,34,35,56,57] Such a complex is not observed in the present case. This observation clearly shows that silica does not simply act as a template to host the same catalytic phase that would be formed in its absence, but plays an active role in the construction of the catalyst.

Interestingly, in the presence of the magnesium precursor only (in the same amount), no diffraction peaks are observed in the XRPD pattern (Figure 1, curve 1). This suggests that in the presence of the titanium phase, the dispersion of the Mg phase on silica decreases. To further clarify this phenomenon, a different bimetallic precatalyst was prepared by following a double impregnation method: the magnesium chloride tetrahydrofuranate precursor was added first, followed by impregnation of the titanium precursor. The resulting XRPD pattern (not reported) was the same as for the SiO_2/TiMg sample prepared via a single impregnation procedure. Thus, we conclude that the titanium chloride tetrahydrofuran precursor has a better affinity toward the silica than the magnesium precursor. However, the XRPD data do not give any information about the localization of the $TiCl_x$ phase on the silica surface and its eventual interaction with the $MgCl_x$ phase in the SiO_2/TiMg precatalyst.

Addition of TOAl to the precatalyst causes a remarkable change in the diffraction pattern (Figure 1, curve 3): the peaks identifying the crystalline magnesium-containing phase are no longer observed, and only the broad halo due to amorphous silica remains. Hence, we conclude that the cocatalyst interacts strongly with the silica-supported $MgCl_x$ phase. Again, no information can be obtained on the structure of the active $TiCl_x$ phase.

Vibrational Properties. Successively, FT-IR spectroscopy was employed to investigate the vibrational properties of both the precatalyst and the catalyst. Indeed, FT-IR spectroscopy is a precious technique to evaluate the occurrence of Ti grafting through surface ≡SiOH groups, as previously demonstrated by some of us for the single phase SiO_2/Ti sample,[47] and as reported in the literature for the similar $SiO_2/TiCl_4$ system,[58−63] and for several organometallic complexes of general formula X_xML_n (where M = transition metal, X = halogen, and L = ligand).[64−71]

The FT-IR spectrum of SiO_2/TiMg precatalyst is shown in Figure 2 (curve 2) in the whole mid-IR (part a) and far-IR (part

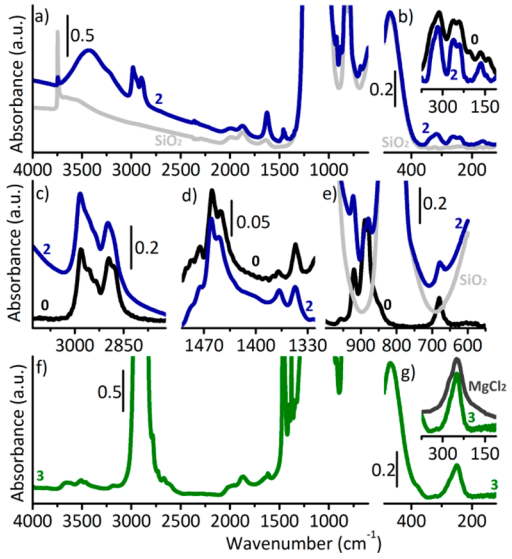

Figure 2. (a, b) Mid- and far-IR spectra of SiO_2/TiMg (curve 2) compared with those of bare SiO_2. A magnification of the far-IR region is displayed in the inset of part b, where the spectrum of the magnesium precursor (curve 0) is also shown. (c−e) Magnifications of the spectral regions where the main absorption bands characteristic of thf vibrations appear. The spectrum of the magnesium precursor is also shown for comparison (curve 0). Same color code as in parts a, b. (f, g): Mid-IR and far-IR spectra of SiO_2/TiMg/TOAl (curve 3). A magnification of the far-IR region is displayed in the inset of part g, where the spectrum of crystalline $MgCl_2$ is also shown.

b) regions, in comparison with that of dehydroxylated silica (curve SiO_2). The two spectra are dominated by the intense bands due to Si−O vibrational modes of the silica framework (1400−950 cm^{-1}) and by their overtone modes (2100−1550 cm^{-1} region).[72] The sharp absorption band observed at 3746 cm^{-1} in the spectrum of pure silica, which is due to isolated surface silanol groups, is almost completely consumed in the spectrum of SiO_2/TiMg. A fraction of the free silanols has been consumed because of titanium grafting, as testified by the presence in the spectrum of SiO_2/TiMg of two broad bands around 925 and 675 cm^{-1}, which are quite evident in narrow frequency regions of transparency. These bands were previously assigned to perturbation of the Si−O framework modes due to titanium grafting.[59,60,62] Moreover, the consumption of the free surface silanols in the spectrum of SiO_2/TiMg is also associated with the appearance of a broad absorption band centered around 3425 cm^{-1}, which can be explained in terms of ν(OH) of ≡SiOH species hydrogen-bonded to a ligand acting as a Lewis base (either a partially uncoordinated titanium sites or thf itself). The corresponding δ(OH) absorption band is

DOI: 10.1021/acscatal.5b01108
ACS Catal. 2015, 5, 5586−5595

observed around 1630 cm^{-1}. This result is different from that found for the single phase SiO_2/Ti sample, in which only the grafting of the titanium precursor was observed.[47]

In addition, the spectrum of SiO_2/TiMg shows narrow absorption bands characteristic of thf vibrational modes[73] in the regions 3050−2800 cm^{-1} (CH_2 stretching; Figure 2c), 1500−1300 cm^{-1} (bending, wagging, and twisting modes; Figure 2d), and 1100−600 cm^{-1} (C−O−C bending modes; Figure 2e). Comparison with the IR spectrum (collected in ATR mode) of the magnesium chloride tetrahydrofuranate precursor (curve 0) provides evidence that most of the thf present in the sample is attached to magnesium sites rather than to titanium sites. Indeed, the vibrational modes of thf ligands (especially those in the 1100−600 cm^{-1} wavenumber region) are very sensitive to the Lewis acidity of the metal center to which they are bonded.[7,56] In addition, in the far-IR region, the spectrum of SiO_2/TiMg closely resembles that of the magnesium precursor, characterized by a complex series of absorption bands at least partially related to Mg−Cl vibrations.

Summarizing, FT-IR spectroscopy suggests that (i) the titanium precursor is mostly grafted to the silica support through surface ≡SiOH groups, as already found for the single-phase SiO_2/Ti sample; (ii) at least a fraction of the magnesium precursor remains unaltered on the silica surface (same vibrational properties), in agreement with the XRPD data (Figure 1, curve 2); and (iii) thf is still present in a large amount, but mainly bonded to the $MgCl_x$ phase.

The IR spectrum of the SiO_2/TiMg/TOAl catalyst (curve 3 in Figure 2f) is remarkably different from that of the precatalyst (curve 2 in Figure 2a−e) in the entire investigated wavenumber region. In particular, (i) the whole spectrum is flattened (the interparticle scattering of light decreases because the pellet is wet); (ii) the broad absorption band in the ν(OH) region completely disappears; (iii) the spectrum is dominated by the intense (and out-of-scale) absorption bands due to $\nu(CH_x)$ (3000−2800 cm^{-1}) and $\delta(CH_x)$ (1500−1300 cm^{-1}) vibrational modes characteristic of TOAl and of the heptane solvent; (iv) unfortunately, nothing can be said about the destiny of thf because the corresponding absorption bands fall in wavenumber regions obscured by the previously mentioned intense bands; and (v) finally, in the far-IR region (Figure 2g), the complex absorption bands due to the magnesium chloride tetrahydrofuranates phase disappear and are substituted by a well-defined band centered at 250 cm^{-1}, which is assigned to $MgCl_2$ (compare curve 3 with the spectrum of a $MgCl_2$ reference, inset in Figure 2g). Therefore, it is possible to conclude that TOAl has a profound effect on the silica-supported $MgCl_x$ phase (in agreement with XRPD data, Figure 1, curve 3) in that it removes most of the thf ligands and promotes the formation of a highly dispersed $MgCl_2$ phase not detected by XRPD but quite visible in the far-IR spectrum.

Titanium Oxidation State and Local Symmetry. The electronic properties of the SiO_2/TiMg precatalyst and the corresponding SiO_2/TiMg/TOAl catalyst were investigated by means of DR UV−vis and Ti K-edge XANES spectroscopy. The DR UV−vis spectra are dominated by the electronic properties of the Ti-containing phase, whereas the $MgCl_x$ phase is expected to contribute in the far-UV region. Ti K-edge XANES spectroscopy is an element-selective technique and as such provides information on the titanium sites only. Both techniques are sensitive to titanium oxidation state and local symmetry.[5,7,74]

The DR UV−vis and normalized XANES spectra of the precatalyst (curves 2 in Figure 3a and b, respectively) are very

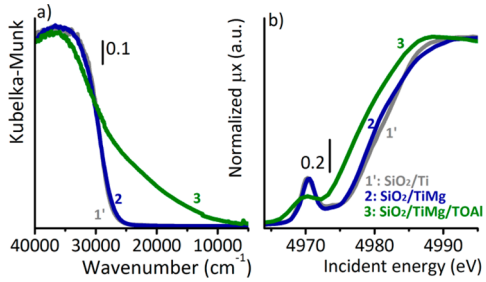

Figure 3. Diffuse reflectance UV−vis spectra in Kubelka−Munk units (part a) and normalized XANES spectra (part b) of SiO_2/Ti (curve 1′), SiO_2/TiMg (curve 2), and SiO_2/TiMg/TOAl (curve 3).

similar to those of the single phase SiO_2/Ti sample previously investigated (curves 1′).[47] This observation provides strong evidence that the titanium sites do have the same formal oxidation state (i.e., 4+) and a similar coordination in the two cases (i.e., on average, 6-fold coordination, where most of the chlorine ligands originally surrounding the titanium sites are substituted by oxygen ligands upon grafting onto silica). In more detail, the intense edge observed in the UV−vis spectra around 30 000 cm^{-1} is due mainly to O → Ti charge-transfer transition.[5,74,75] The pre-edge peak observed around 4970 eV in the XANES spectra is assigned to 1s → 3pd transitions.[5,47,75] The low intensity of this peak (∼0.2 in normalized absorption) is indicative of a high coordination, in agreement with UV−vis data. Both pre-edge and edge regions are quite broad, indicating a large heterogeneity of titanium sites.

Addition of TOAl causes significant changes in both DR UV−vis and XANES spectra, which signify a reduction of the titanium sites. In particular, in the UV−vis spectrum, a broad and unstructured absorption appears in the visible region, where d−d transitions characteristic of Ti^{3+} sites in a 6-fold coordination are expected to occur.[76] Simultaneously, the intense edge in the charge-transfer region becomes broader and shifts at higher wavenumber values. In the XANES spectra, the absorption edge shifts toward lower energy (from 4979 to 4977 eV, as evaluated at the maximum of the derivative spectra), as expected for reduction of Ti^{4+} to Ti^{3+}; simultaneously, the pre-edge peak decreases in intensity, becomes broader, and slightly shifts at lower energy. In summary, both UV−vis and XANES spectra demonstrate that TOAl reduces the Ti^{4+} sites originally grafted at the SiO_2 surface to a large variety of Ti^{3+} sites, as expected on the basis of the specialized literature.[1,2]

Local Structure around Titanium Sites and Ligands Identification. The broad character of both DR UV−vis and Ti K-edge XANES spectra does not allow extraction of precise information on the nature of the titanium phase in either the precatalyst or the catalyst. For this reason, we turned our attention to two element-selective spectroscopic techniques (EXAFS and vtc-XES) whose potential in characterizing the type of ligands and the local structure of transition metals on inorganic matrixes has been largely demonstrated in the past.[5,11,44]

The phase-uncorrected Fourier transform (FT) of the $k^3\chi(k)$ EXAFS function for the SiO_2/TiMg precatalyst is shown in Figure 4 (curve 2) in both modulus and imaginary parts (parts a and b, respectively) in comparison with that of the single-phase SiO_2/Ti sample (curve 1′), which was discussed in our

DOI: 10.1021/acscatal.5b01108
ACS Catal. 2015, 5, 5586−5595

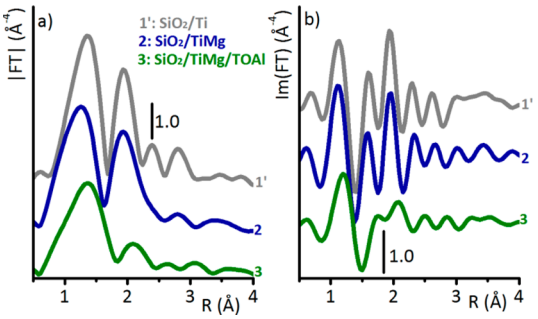

Figure 4. Phase-uncorrected Fourier-transform (in both modulus and imaginary parts, parts a and b, respectively) of the k^3-weighted $\chi(k)$ EXAFS function for SiO_2/Ti (curve 1′), SiO_2/TiMg (curve 2), and SiO_2/TiMg/TOAl (curve 3). The spectra were extracted in the Δk = 2.0−10.0 $Å^{-1}$ range and vertically translated for clarity.

previous work.[47] Both spectra are dominated by two main contributions centered around 1.4 and 2.0 Å, respectively (values not phase-corrected), which were assigned to the copresence of oxygen and chlorine ligands around the titanium site. The similarity of the two spectra provides evidence that the local structure around the titanium sites is comparable in the two samples, in agreement with DR UV−vis and XANES data. Hence, the presence of the $MgCl_x$ phase seems to have a minor effect in influencing the local structure of the titanium sites in the precatalyst, which are grafted to the silica surface mostly through Ti−O bonds.

The FT of the EXAFS spectrum for the catalyst obtained after the interaction of the precatalyst with TOAl is substantially different, demonstrating that some changes occurred in the local structure of the titanium sites. In particular, the spectrum of the catalyst is less intense than that of the precatalyst and is dominated by a first shell signal centered around 1.4 Å (with a shoulder around 1.0 Å), whereas the signal at the longer distance characteristic of chlorine ligands has almost disappeared (particularly evident in the imaginary part). Hence, from a qualitative analysis of the EXAFS spectrum, it might be suggested that upon interaction of the precatalyst with TOAl, most of the titanium sites remain attached to the silica surface, and the few chlorine ligands originally present are removed. However, the data discussed above demonstrate that activation by TOAl promotes the formation of a highly dispersed $MgCl_2$ phase. In the presence of such an important structural rearrangement, one must take into account the possibility that the titanium phase may be detached from the silica surface and may interact with $MgCl_2$, mimicking what happens for heterogeneous $MgCl_2$-based Ziegler−Natta catalysts.

Unfortunately, a quantitative analysis of the EXAFS spectra was heavily affected by problems intrinsic to the nature of the analyzed sample, and possibly common to other systems. The main problemas are related to (i) the relatively short k-range that can be safely used in the analysis and (ii) to the presence in the titanium coordination sphere of several ligands at similar coordination distances, whose contribution is at least partially out-of-phase.

This means that any quantitative evaluation of the titanium coordination numbers is simply not meaningful and, at most, only coordination distances can be determined. An example of the problems encountered in the data analysis is discussed below for the SiO_2/TiMg/TOAl catalyst. Different strategies were followed to fit the experimental spectrum, as summarized in Table 2. Figure 5 shows the best fits overlapped to the experimental data and the separate contributions of different ligands to the fits.

Table 2. Optimized Parameters in the Analysis of the EXAFS Spectrum for the SiO_2/TiMg/TOAl According to Three Different Structural Models of Increasing Complexity[a]

variables	FIT 1[b]	FIT 2[c]	FIT 3[d]
ΔE (eV)	−6 ± 3	−4 ± 3	−4 ± 2
N_O	3.2 ± 1.0	3.3 ± 0.9	1.1 ± 0.5
R_O (Å)	1.90 ± 0.03	1.92 ± 0.02	1.84 ± 0.02
σ_O^2 ($Å^2$)	0.019 ± 0.006	0.019 ± 0.006	0.007 ± 0.005
N_{Clt}			1.8 ± 0.6
R_{Clt} (Å)			2.18 ± 0.03
σ_{Clt}^2 ($Å^2$)			0.013 ± 0.003
N_{Clb}		0.3 ± 0.4	1.8 ± 0.6
R_{Clb} (Å)		2.46 ± 0.03	2.43 ± 0.03
σ_{Clb}^2 ($Å^2$)		0.005 ± 0.014	0.013 ± 0.003
R_{factor}	0.06	0.02	0.01

[a] $N_{ind} = 2\Delta k \Delta R/\pi > 10$. [b] FIT 1 was performed by considering the contribution of only oxygen ligands. [c] FIT 2 considered the presence of two type of ligands: oxygen and chlorine (Cl_b = bridged chlorine). [d] FIT 3 was done by adding to the model used in FIT 2 the contribution from a second type of chlorine ligand (Cl_t = terminal chlorine) at shorter distance.

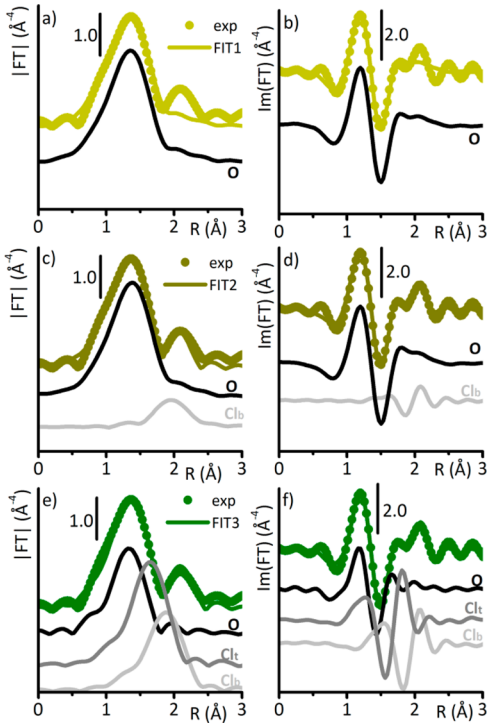

Figure 5. Analysis of the EXAFS spectrum for the SiO_2/TiMg/TOAl catalyst. (a, b) FIT 1, which includes the contribution of only oxygen ligands. The experimental phase-uncorrected FT of the $k^3\chi(k)$ EXAFS function is shown in both modulus and imaginary parts (dotted curves in parts a and b, respectively), overlapped to the result of the fit (solid lines). The contributions of the oxygen ligands is also shown, vertically translated for clarity. (c, d) Same as for FIT 2, which includes the contributions of oxygen and chlorine (Cl_b) ligands. (e, f) Same as for FIT 3, which includes an additional chlorine ligand at shorter distance (Cl_t). The results of the three fits are summarized in Table 2.

DOI: 10.1021/acscatal.5b01108
ACS Catal. 2015, 5, 5586−5595

A first fit (FIT 1 in Table 2 and Figure 5a and b) was attempted by including the contribution of oxygen only. The fit was performed by optimizing the following parameters: (i) ΔE_0; (ii) the coordination number (N_O), which was renormalized to the S_0^2 value obtained by fitting the signal of TiO_2 reference compound; (iii) the Ti−O distance; (iv) the Debye−Waller factor (σ_O^2). The results are summarized in Table 2: on average, each titanium atom is surrounded by 3.2 ± 1.0 oxygen ligands at a distance of R_O = 1.90 ± 0.03 Å, with a quite large Debye−Waller factor (σ_O^2 = 0.019 ± 0.006 Å^2). Although the coordination distance looks reasonable, the number of ligands is clearly underestimated. The fit is obviously unable to reproduce the experimental signal in the 2.0−3.0 Å region, which is due to at least one additional coordination shell overlooked in the model of FIT 1. This problem is considered in FIT 2. However, the results do not greatly change by considering the copresence of oxygen and chlorine ligands (Cl_b = bridged chlorine), which may be present if the titanium-containing phase interacts with the highly dispersed $MgCl_2$ phase. FIT 2 (Figure 5d) was performed by optimizing the following parameters: (i) a single ΔE_0, common to the two scattering paths; (ii) the coordination numbers for both ligands (N_O and N_{Clb}), renormalized to the S_0^2 values obtained by fitting the signals of TiO_2 and α-$TiCl_3$ reference compounds; (iii) the two Ti−L distances (L = ligand); (iv) the two Debye−Waller factors for the two ligands. According to the fit, on average, each titanium atom has only 3.6 ligands, which is incompatible with the other available experimental data.

A third fit (FIT 3 in Table 2 and Figure 5e, f) was then performed by considering, in addition to the two ligands used in FIT 2, the presence of a second type of chlorine ligands (Cl_t = terminal chlorine) at a distance shorter than Cl_b. It is worth noticing that the copresence of terminal and bridged chlorine ligands (at shorter and longer distances, respectively) in the titanium coordination sphere was recently reported by some of us for analogous Ziegler−Natta catalysts not silica-supported.[8] The agreement with the experimental data is better than FIT 2 (R_{factor} in Table 2). In this case, the coordination numbers are completely reversed: 1.1 ± 0.5 oxygen ligands at a distance of R_O = 1.84 ± 0.02 Å (with σ_O^2 = 0.007 ± 0.005 Å^2), 1.8 ± 0.6 chlorine ligands at a distance of R_{Clt} = 2.18 ± 0.03 Å, and 1.8 ± 0.6 chlorine ligands at a distance of R_{Clb} = 2.43 ± 0.03 Å (with σ_{Cl}^2 = 0.013 ± 0.003 Å^2). The results of this fit are more realistic. On average, each titanium site has about 5 ligands, which is compatible with previously discussed results and also with some of the widely accepted models for titanium active sites in $MgCl_2$-supported Ziegler−Natta catalysts. It is important to observe that the Debye−Waller factors for the chlorine ligands are quite large, accounting for a large heterogeneity of species.

We might speculate on the presence of one available coordination vacancy around the titanium sites, which would be predictable on the basis of the models proposed for titanium sites in classical ($MgCl_2$-supported) Ziegler−Natta catalysts. We might also hazard the hypothesis that the low-Z element detected by EXAFS is not an oxygen ligand, but rather, a carbon ligand (EXAFS is unable to distinguish among oxygen and carbon ligands), as expected by assuming the Cosse−Arlman mechanism for formation of active sites.[77] Nevertheless, it is common opinion that the catalytically active titanium sites are only a few of the total. Hence, it appears safer to interpret the EXAFS results in terms of copresence of two different phases: a minor fraction of isolated titanium sites still grafted to silica, and a $TiCl_x$ phase in which different titanium sites are bridged through chlorine ligands to a highly dispersed, silica-supported, $MgCl_2$ phase. The active titanium sites bearing an alkyl ligand, if present, may be easily hidden by these two phases.

In contrast to EXAFS, vtc-XES spectroscopy does not suffer from interference problems, and it is a valuable technique for ligand identification.[78−80] The vtc-XES spectrum of SiO_2/TiMg precatalyst is compared in Figure 6 with that of the single phase

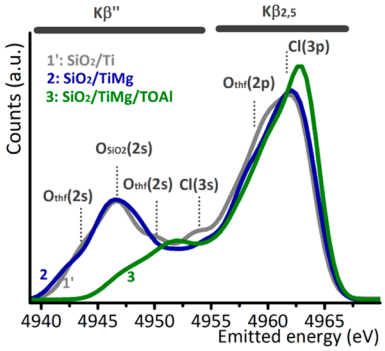

Figure 6. Normalized vtc-XES spectra of SiO_2/Ti (curve 1′), SiO_2/TiMg (curve 2) and SiO_2/TiMg/TOAl (curve 3). The Kβ'' and K$\beta_{2,5}$ regions are indicated on the top, and the main features identifying oxygen and chlorine ligands are labeled.

SiO_2/Ti sample, discussed in our previous work;[47] the assignment of the Kβ'' and K$\beta_{2,5}$ fluorescence lines is also reported. It is useful to recall that Kβ'' fluorescence lines are due to transitions involving mainly molecular orbitals with ligand s-atomic character, and thus, they are useful for ligand identification, whereas K$\beta_{2,5}$ fluorescence lines are due to transitions involving primarily molecular orbitals having a ligand p-atomic character, and hence, they are sensitive to the valence orbitals.

The vtc-XES spectrum of SiO_2/TiMg (curve 2) is very similar to that of SiO_2/Ti (curve 1′), confirming once more that the local structure and the electronic state of the titanium sites is similar in the two samples. Also in the SiO_2/TiMg precatalyst, the titanium sites are grafted to silica through some oxygen ligands (identified by the intense Kβ'' line centered at 4947 eV) and retain in the coordination sphere a few chlorine ligands (identified by the Kβ'' line at 4954 eV) and a few thf ligands (Kβ'' lines at 4943 and 4950 eV). However, a better comparison allows one to observe that the Kβ'' lines assigned to a transition involving mainly molecular orbitals lying on thf ligands are shifted to lower energy in the spectrum of the precatalyst. Although the increased complexity of the system makes a systematic investigation (as presented in our previous work)[47] not feasible, preliminary DFT calculations[81] proved that the shift of the Kβ'' lines assigned to thf ligands can be reproduced by considering open thf ligands. This means that the presence of the magnesium phase on the silica surface adjacent to the grafted titanium sites has an influence on the stability of the thf ligands. It is interesting to observe that experimental evidence, supported by DFT calculations, for opening of thf with the consequent formation of titanium alkoxy surface species has been provided recently for a similar $MgCl_2$/thf/$TiCl_4$ system.[29]

The vtc-XES spectrum of the SiO_2/TiMg/TOAl catalyst is substantially different from that of the precatalyst, demonstrating that the activator drastically affects the local structure of the

DOI: 10.1021/acscatal.5b01108
ACS Catal. 2015, 5, 5586−5595

titanium sites, in agreement with EXAFS data. In particular, in the Kβ'' region:

(i) The lines identifying the thf ligand are no longer present, providing evidence that most of the thf (also the opened one) has been displaced by TOAl from the titanium sites, in good agreement with previous literature about activation of commercial silica-supported Ziegler–Natta catalysts containing thf or other electron donors.[1,2]

ii) The band at 4947 eV characteristic of oxygen belonging to silica is much less intense, suggesting that most of the titanium sites are no longer grafted to silica. This evidence agrees with the low coordination number of the Ti–O shell found in FIT 3 of the EXAFS data (see Table 1).

iii) A new and quite visible band appears around 4952 eV. A similar band was recently observed by some of us in the vtc-XES spectrum of a similar, not silica-supported, TiMg/TOAl catalyst, although it was much less intense.[8] The energy position of this band is compatible both with carbon ligands (that might be present according to the Cossee–Arlman mechanism for active sites formation[77]) and with bridged-chlorine ligands, whose presence is supported by the data discussed above.

In the K$\beta_{2,5}$ region, the line assigned to the thf ligand disappears, whereas the band characteristic of chlorine ligands increases in intensity and becomes sharper, in close similarity to the spectrum of the violet $TiCl_3$ reference compound.[8]

Summarizing, the whole set of EXAFS and vtc-XES data provide evidence that the local structure around the titanium sites is totally reconstructed after the interaction of the precatalyst with TOAl. A consistent fraction of titanium sites has chlorine ligands in the first coordination sphere, demonstrating that they are mainly detached from the silica surface and interact with a highly dispersed $MgCl_2$ phase whose presence was clearly revealed by far-IR spectroscopy. According to EXAFS data analysis, two types of chlorine ligands are present: terminal chlorine species at shorter distance (2.18 ± 0.03 Å) and bridged chlorine species at longer distance (2.43 ± 0.03 Å). Vtc-XES data might be compatible with the presence of a few titanium sites bearing an alkyl ligand, but definitive proof is still missing.

3.2. In Situ Ethylene Polymerization. Finally, we tested the SiO_2/TiMg/TOAl catalyst in ethylene polymerization. The catalytic performances of this commercial catalyst are reported in the specialized literature for gas-phase ethylene polymerization conducted in a fluidized bed reactor.[32−38] However, it is of paramount importance to verify that the activation conditions adopted during the spectroscopic investigation of the SiO_2/TiMg/TOAl system lead to a catalyst active in ethylene polymerization. To this aim, we monitored ethylene polymerization at room temperature by in situ FT-IR spectroscopy, following the same approach extensively used to investigate the initial steps of ethylene polymerization on the Phillips catalyst.[5,44−46,82−85] The presence of the aluminum alkyl activator and of the solvent prevented up to now the exploitation of the same method to follow in situ olefin polymerization on industrially relevant Ziegler–Natta catalysts. To the best of our knowledge, the only FT-IR spectra showing in situ ethylene polymerization on Ziegler–Natta catalysts were collected in ATR mode on a planar model of Ziegler–Natta catalyst.[25]

We found that a thin pellet of the SiO_2/TiMg/TOAl catalyst, obtained upon impregnation of a thin pellet of the SiO_2/TiMg precatalysts with the TOAl/heptane solution (exactly following the same procedure used during the previous spectroscopic investigations, Al/Ti ∼ 10), is measurable by FT-IR spectroscopy in transmission (Figure 2f), although most of the spectral regions were obscured by the intense and out-of-scale absorption bands due to TOAl, to the solvent and to the reaction byproducts (e.g., $Al(Oct)_2Cl$). In our prospect, the presence of liquid TOAl/heptane in the silica pores may simulate, if not industrially significant polymerization conditions, at least prepolymerization conditions (in which the monomer is fed onto the catalyst in the presence of the activator and the solvent at low pressure and low temperature), simultaneously allowing performance of in situ FT-IR experiments in transmission mode. To separate the vibrational manifestation of the polymer from those of the activator, we worked with deuterated ethylene (ethylene-*d*). As anticipated in the Experimental section, the experimental procedure is crucial. In particular, a partial removal of the solvent (upon degassing the reaction cell) was found to have a negative effect, probably enhancing the catalyst deactivation. In contrast, in the presence of the solvent, polymerization readily takes place, already at low ethylene pressure and at room temperature.

A typical experiment is shown in Figure 7a in the whole frequency range, whereas Figure 7b shows an enlargement of

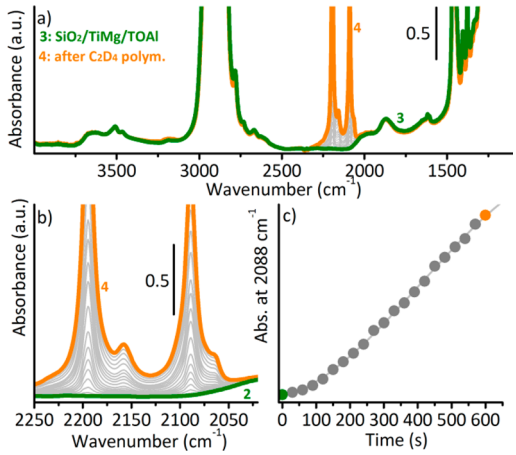

Figure 7. (a) FT-IR spectra collected during polymerization of C_2D_4 (room temperature, $P_{C_2D_4}$ = 100 mbar) on the SiO_2/TiMg/TOAl catalyst. Curve 3, spectrum of the catalyst before interaction with C_2D_4; curve 4, after 10 min of C_2D_4 polymerization. Gray spectra were collected at regular time intervals during polymerization. (b) Enlargement of the spectral region where the absorption bands characteristic of dPE appear. (c) Intensity of the absorption band at 2088 cm^{-1} as a function of time.

the spectral region characteristic of polyethylene-*d*. Upon ethylene-*d* admission in the reaction cell (room temperature, $P_{C_2D_4}$ = 100 mbar), two intense absorption bands gradually grow at 2195 and 2089 cm^{-1}, which are assigned to $\nu_{asym}(CD_2)$ and $\nu_{sym}(CD_2)$ vibrational modes of the polyethylene-*d* chains. Another two weaker bands are observed at 2158 and 2065 cm^{-1} that are assigned to the 2δ (CD_2) mode (fundamental vibration around 1085 cm^{-1}) and to the combination of δ (CD_2) + 2ρ (CD_2) (fundamental $\rho(CD_2)$ mode around 520 cm^{-1}). Figure 7c shows a plot of the intensity of the IR band at 2088 cm^{-1} (chosen here as a reference band to monitor the polymer

DOI: 10.1021/acscatal.5b01108
ACS Catal. 2015, 5, 5586−5595

growth) versus time. After a short induction period (~60 s), which is likely due to the diffusion of the monomer into the liquid TOAl/heptane phase, an almost linear dependence is observed within the investigated time interval, and no evidence of catalyst deactivation was observed. It is worth noticing that these data do not give any quantitative information on the kinetics of the reaction, but rather demonstrate that it is possible to look at a silica-supported Ziegler–Natta catalyst in action by means of spectroscopic techniques. This is not a trivial job for most of the heterogeneous catalysts, and it has been precluded so far for Ziegler–Natta catalysts.

4. CONCLUSIONS

The structural, vibrational and electronic properties of an industrially relevant, silica-supported, Ziegler–Natta catalyst were investigated by a large arsenal of characterization techniques during all the steps of catalyst preparation, including precatalyst activation and ethylene polymerization. It was demonstrated that the alkyl–aluminum activator significantly reconstructs the whole precatalyst, acting on all the catalyst constituents and not only on the $TiCl_x$ phase. In particular, it was found that TOAl removes most of the thf originally present in the precatalyst and promotes the formation of a $MgCl_2$ phase highly dispersed on the silica surface, not detected by XRD but identified by means of far-IR spectroscopy. Simultaneously, the titanium sites get reduced. Although we cannot be fully quantitative on the number of titanium sites that are reduced by TOAl, the profound modifications observed with all the employed techniques do suggest that the reduction process involves most of the titanium sites in the precatalyst. Most of them detach from the silica surface to form $TiCl_x$ species connected to the silica-supported $MgCl_2$ phase through bridging chlorine ligands and characterized by the presence of terminal chlorine ligands at shorter distances. Hence, the final catalytic phase would resemble that formed in the absence of silica, although probably much more dispersed.

Although at present, we cannot distinguish between active and spectator sites, the herein reported data are among the few experimental evidence on the structure of the titanium sites at a molecular scale in industrially significant silica-supported Ziegler–Natta catalysts. Finally, and very important, the same catalyst was observed by means of FT-IR spectroscopy during ethylene polymerization in the presence of the activator, solvent, and monomer. These results definitely validate the step-by-step synthetic approach used in this work and open interesting perspectives in the field of in situ investigation of Ziegler–Natta catalysts in action in industrially significant polymerization conditions. We believe that a systematic investigation of all the catalyst's components by means of a multitechnique approach (as proposed in this work) might be the first fundamental step toward understanding their mutual interactions and functions down to a level of detail rarely reached by other methods, making the design of these catalysts a realistic goal for the future.

AUTHOR INFORMATION

Corresponding Author

*E-mail: elena.groppo@unito.it.

Notes

The authors declare no competing financial interest.

ACKNOWLEDGMENTS

C.L. thanks the Mega-grant of the Russian Federation Government to support scientific research at the Southern Federal University, No. 14.Y26.31.0001. We are grateful to Wim Bras (BM26 at ESRF), Roelof van Silfhout, and Anton Kachatkou (The University of Manchester) for the fruitful collaboration during the XAS measurements and Pieter Glatzel, Mauro Rovezzi, and Christophe Lapras (ID26 at ESRF) for help during the XES experiments. We are indebted to Harald Muller (Chemical Lab at ESRF) for providing us the indispensable and always perfect glovebox during the experiments at ESRF. We would like to thank Francesco Masi for the valuable discussion from an industrial perspective and Prof. Adriano Zecchina for his everyday dialog and constant encouragement.

REFERENCES

(1) Albizzati, E.; Giannini, U.; Collina, G.; Noristi, L.; Resconi, L. Catalysts and Polymerizations. In *Polypropylene Handbook*; Moore, E. P. J., Ed.; Hanser-Gardner Publications: Cincinnati, OH, 1996.
(2) Busico, V. *MRS Bull.* **2013**, *38*, 224–228.
(3) Klapper, M.; Joe, D.; Nietzel, S.; Krumpfer, J. W.; Müllen, K. *Chem. Mater.* **2014**, *26*, 802–819.
(4) Busico, V. *Dalton Trans.* **2009**, 8794–8802.
(5) Groppo, E.; Seenivasan, K.; Barzan, C. *Catal. Sci. Technol.* **2013**, *3*, 858–878.
(6) Dwivedi, S.; Taniike, T.; Terano, M. *Macromol. Chem. Phys.* **2014**, *215*, 1698–1706.
(7) Seenivasan, K.; Sommazzi, A.; Bonino, F.; Bordiga, S.; Groppo, E. *Chem.—Eur. J.* **2011**, *17*, 8648–8656.
(8) Groppo, E.; Gallo, E.; Seenivasan, K.; Lomachenko, K. A.; Sommazzi, A.; Bordiga, S.; Glatzel, P.; Van Silfhout, R.; Kachatkou, A.; Bras, W.; Lamberti, C. *ChemCatChem* **2015**, *7*, 1432–1437.
(9) Lamberti, C.; Groppo, E.; Spoto, G.; Bordiga, S.; Zecchina, A. *Adv. Catal.* **2007**, *51*, 1–74.
(10) Lamberti, C.; Zecchina, A.; Groppo, E.; Bordiga, S. *Chem. Soc. Rev.* **2010**, *39*, 4951–5001.
(11) Bordiga, S.; Groppo, E.; Agostini, G.; Van Bokhoven, J. A.; Lamberti, C. *Chem. Rev.* **2013**, *113*, 1736–1850.
(12) Frenkel, A. I.; Rodriguez, J. A.; Chen, J. G. *ACS Catal.* **2012**, *2*, 2269–2280.
(13) Lysova, A. A.; Koptyug, I. V. *Chem. Soc. Rev.* **2010**, *39*, 4585–4601.
(14) Schoonheydt, R. A. *Chem. Soc. Rev.* **2010**, *39*, 5051–5066.
(15) Tromp, M. *Philos. Trans. R. Soc. A Math. Phys. Eng. Sci.* **2015**, *373*, 20130152.
(16) Vimont, A.; Thibault-Starzyk, F.; Daturi, M. *Chem. Soc. Rev.* **2010**, *39*, 4928–4950.
(17) Wachs, I. E.; Roberts, C. A. *Chem. Soc. Rev.* **2010**, *39*, 5002–5017.
(18) Zaera, F. *Chem. Soc. Rev.* **2014**, *43*, 7624–7663.
(19) van Bokhoven, J. A.; Lamberti, C. X-ray absorption and emission spectroscopy for catalysis. In *X-Ray Absorption and X-ray Emission Spectroscopy: Theory and Applications*; van Bokhoven, J. A., Lamberti, C., Ed.; John Wiley & Sons: New York, 2015; Vol. 2.
(20) McKenna, T. F. L.; Tioni, E.; Ranieri, M. M.; Alizadeh, A.; Boisson, C.; Monteil, V. *Can. J. Chem. Eng.* **2013**, *91*, 669–686.
(21) Oleshko, V. P.; Crozier, P. A.; Cantrell, R. D.; Westwood, A. D. *Macromol. Rapid Commun.* **2001**, *22*, 34–40.
(22) Andoni, A.; Chadwick, J. C.; Niemantsverdriet, H. J. W.; Thune, P. C. *Macromol. Rapid Commun.* **2007**, *28*, 1466–1471.
(23) Andoni, A.; Chadwick, J. C.; Milani, S.; Niemantsverdriet, H.; Thune, P. C. *J. Catal.* **2007**, *247*, 129–136.
(24) Andoni, A.; Chadwick, J. C.; Niemantsverdriet, H. J. W.; Thune, P. C. *J. Catal.* **2008**, *257*, 81–86.
(25) Andoni, A.; Chadwick, J. C.; Niemantsverdriet, J. W.; Thune, P. C. *Catal. Lett.* **2009**, *130*, 278–285.

DOI: 10.1021/acscatal.5b01108
ACS Catal. 2015, 5, 5586–5595

(26) Morra, E.; Giamello, E.; Van Doorslaer, S.; Antinucci, G.; D'Amore, M.; Busico, V.; Chiesa, M. *Angew. Chem., Int. Ed.* **2015**, *54*, 4857−4860.
(27) Giannini, U.; Albizzati, E.; Parodi, S.; Pirinoli, F. *Catalysts for polymerizing olefins*. U.S. Patent 4,124,532, November 7, 1978.
(28) Sobota, P.; Utko, J.; Lis, T. *J. Chem. Soc., Dalton Trans.* **1984**, 2077−2079.
(29) Grau, E.; Lesage, A.; Norsic, S.; Copéret, C.; Monteil, V.; Sautet, P. *ACS Catal.* **2013**, *3*, 52−56.
(30) Pirinen, S.; Koshevoy, I. O.; Denifl, P.; Pakkanen, T. T. *Organometallics* **2013**, *32*, 4208−4213.
(31) Pirinen, S.; Jayaratne, K.; Denifl, P.; Pakkanen, T. T. *J. Mol. Catal. A: Chem.* **2014**, *395*, 434−439.
(32) Goeke, G. L.; Wagner, B. E.; Karol, F. J. *Impregnated polymerization catalyst, process for preparing and use for ethylene copolymerization*. U.S. Patent 4,302,565, 1981.
(33) Karol, F. J.; Goeke, G. L.; Wagner, B. E.; Fraser, W. A.; Jorgersen, R. J.; Friis, N. *Preparation of ethylene copolymers in fluid bed reactors*. U.S. Patent 4,302,566, 1981.
(34) Karol, F. J. *Catal. Rev.: Sci. Eng.* **1984**, *26*, 557.
(35) Karol, F. J.; Cann, K. J.; Wagner, B. E. In *Transition Metals and Organometallics as Catalysts for Olefin Polymerization*; Kaminsky, W., Sinn, H., Eds.; Springer: Berlin, Germany, 1988; p 149.
(36) Kissin, Y. V. In *Alkene Polymerization Reactions with Transition Metal Catalysts*; Elsevier: Amsterdam, The Netherlands, 2008.
(37) Nowlin, T. E.; Mink, R. I.; Kissin, Y. V. In *Transition Metal Polymerization Catalysts*; Hoff, R., Mathers, R. T., Eds.; John Wiley & Sons: Hoboken, NJ, USA, 2009.
(38) Nowlin, T. E. *Business and Technology of the Global Polyethylene Industry*; Scrivener Publishing LLC: New York, 2014.
(39) Pullukat, T. J.; Hoff, R. E. *Catal. Rev.: Sci. Eng.* **1999**, *41*, 389−428.
(40) Severn, J. R.; Chadwick, J. C.; Duchateau, R.; Friederichs, N. *Chem. Rev.* **2005**, *105*, 4073−4147.
(41) McKenna, T. F. L.; Di Martino, A.; Weickert, G.; Soares, J. B. P. *Macromol. React. Eng.* **2010**, *4*, 40−64.
(42) Lee, M. Y.; Scott, S. L. *Chem.—Eur. J.* **2011**, *17*, 4632−4639.
(43) Campos, J. M.; Lourenço, J. P.; Cramail, H.; Ribeiro, M. R. *Prog. Polym. Sci.* **2012**, *37*, 1764−1804.
(44) Groppo, E.; Lamberti, C.; Bordiga, S.; Spoto, G.; Zecchina, A. *Chem. Rev.* **2005**, *105*, 115−183.
(45) Groppo, E.; Lamberti, C.; Spoto, G.; Bordiga, S.; Magnacca, G.; Zecchina, A. *J. Catal.* **2005**, *236*, 233−244.
(46) Zecchina, A.; Groppo, E. *Proc. R. Soc. London, Ser. A* **2012**, *468*, 2087−2098.
(47) Seenivasan, K.; Gallo, E.; Piovano, A.; Vitillo, J. G.; Sommazzi, A.; Bordiga, S.; Lamberti, C.; Glatzel, P.; Groppo, E. *Dalton Trans.* **2013**, *42*, 12706−12713.
(48) Manxzer, L. E. *Inorg. Synth.* **1982**, *21*, 135−136.
(49) Nikitenko, S.; Beale, A. M.; van der Eerden, A. M. J.; Jacques, S. D. M.; Leynaud, O.; O'Brien, M. G.; Detollenaere, D.; Kaptein, R.; Weckhuysen, B. M.; Bras, W. *J. Synchrotron Radiat.* **2008**, *15*, 632−640.
(50) van Silfhout, R.; Kachatkou, A.; Groppo, E.; Lamberti, C.; Bras, W. *J. Synchrotron Radiat.* **2014**, *21*, 401−408.
(51) Ravel, B.; Newville, M. *J. Synchrotron Radiat.* **2005**, *12*, 537−541.
(52) Zabinsky, S. I.; Rehr, J. J.; Ankudinov, A. L.; Albers, R. C.; Eller, M. J. *Phys. Rev. B: Condens. Matter Mater. Phys.* **1995**, *52*, 2995.
(53) Gallo, E.; Lamberti, C.; Glatzel, P. *Phys. Chem. Chem. Phys.* **2011**, *13*, 19409−19419.
(54) Gallo, E.; Bonino, F.; Swarbrick, J. C.; Petrenko, T.; Piovano, A.; Bordiga, S.; Gianolio, D.; Groppo, E.; Neese, F.; Lamberti, C.; Glatzel, P. *ChemPhysChem* **2013**, *14*, 79−83.
(55) Neese, F. *Wiley Interdiscip. Rev.-Comput. Mol. Sci.* **2012**, *2*, 73−78.
(56) Kim, I.; Chung, M. C.; Choi, H. K.; Kim, J. H.; Woo, S. I. *Stud. Surf. Sci. Catal.* **1990**, *56*, 323−343.
(57) Kim, J. H.; Jeong, Y. T.; Woo, S. I. *J. Polym. Sci., Part A: Polym. Chem.* **1994**, *32*, 2979−2987.
(58) Morrow, B. A.; Hardin, A. H. *J. Phys. Chem.* **1979**, *83*, 3135−3141.
(59) Kinney, J. B.; Staley, R. H. *J. Phys. Chem.* **1983**, *87*, 3735−3740.
(60) Haukka, S.; Lakomaa, E. L.; Jylha, O.; Vilhunen, J.; Hornytzkyj, S. *Langmuir* **1993**, *9*, 3497−3506.
(61) Haukka, S.; Lakomaa, E. L.; Root, A. *J. Phys. Chem.* **1993**, *97*, 5085−5094.
(62) Kytokivi, A.; Haukka, S. *J. Phys. Chem. B* **1997**, *101*, 10365−10372.
(63) Schrijnemakers, K.; Van Der Voort, P.; Vansant, E. F. *Phys. Chem. Chem. Phys.* **1999**, *1*, 2569−2572.
(64) Basset, J. M.; Lefebvre, F.; Santini, C. *Coord. Chem. Rev.* **1998**, *180*, 1703−1723.
(65) Coperet, C.; Chabanas, M.; Petroff Saint-Arroman, R.; Basset, J. M. *Angew. Chem., Int. Ed.* **2003**, *42*, 156−181 and references therein..
(66) Rascon, F.; Wischert, R.; Coperet, C. *Chem. Sci.* **2011**, *2*, 1449−1456.
(67) Gajan, D.; Coperet, C. *New J. Chem.* **2011**, *35*, 2403−2408.
(68) Bini, F.; Rosier, C.; Saint-Arroman, R. P.; Neumann, E.; Dablemont, C.; de Mallmann, A.; Lefebvre, F.; Niccolai, G. P.; Basset, J. M.; Crocker, M.; Buijink, J. K. *Organometallics* **2006**, *25*, 3743−3760.
(69) Tosin, G.; Santini, C. C.; Taoufik, M.; De Mallmann, A.; Basset, J. M. *Organometallics* **2006**, *25*, 3324−3335.
(70) Saint-Arroman, R. P.; Basset, J. M.; Lefebvre, F.; Didillon, B. *Appl. Catal., A* **2005**, *290*, 181−190.
(71) Le Roux, E.; Chabanas, M.; Baudouin, A.; de Mallmann, A.; Coperet, C.; Quadrelli, E. A.; Thivolle-Cazat, J.; Basset, J. M.; Lukens, W.; Lesage, A.; Emsley, L.; Sunley, G. J. *J. Am. Chem. Soc.* **2004**, *126*, 13391−13399.
(72) Ricchiardi, G.; Damin, A.; Bordiga, S.; Lamberti, C.; Spano, G.; Rivetti, F.; Zecchina, A. *J. Am. Chem. Soc.* **2001**, *123*, 11409−11419.
(73) Cadioli, B.; Gallinella, E.; Coulombeau, C.; Jobic, H.; Berthier, G. *J. Phys. Chem.* **1993**, *97*, 7844−7856.
(74) Bordiga, S.; Coluccia, S.; Lamberti, C.; Marchese, L.; Zecchina, A.; Boscherini, F.; Buffa, F.; Genoni, F.; Leofanti, G.; Petrini, G.; Vlaic, G. *J. Phys. Chem.* **1994**, *98*, 4125−4132.
(75) Bordiga, S.; Bonino, F.; Damin, A.; Lamberti, C. *Phys. Chem. Chem. Phys.* **2007**, *9*, 4854−4878.
(76) Figgis, B. N. *Introduction to ligand fields*; John Wiley & Sons: New York, 1966.
(77) Cossee, P. *J. Catal.* **1964**, *3*, 80−88.
(78) Glatzel, P.; Bergmann, U. *Coord. Chem. Rev.* **2005**, *249*, 65−95.
(79) Glatzel, P.; Weng, T.-C.; Kvashnina, K.; Swarbrick, J.; Sikora, M.; Gallo, E.; Smolentsev, N.; Mori, R. A. *J. Electron Spectrosc. Relat. Phenom.* **2013**, *188*, 17−25.
(80) Singh, J.; Lamberti, C.; van Bokhoven, J. A. *Chem. Soc. Rev.* **2010**, *39*, 4754−4766.
(81) Gallo, E., Ph.D. Thesis in Materials Science, University of Turin, Italy, 2013.
(82) Groppo, E.; Lamberti, C.; Bordiga, S.; Spoto, G.; Zecchina, A. *J. Catal.* **2006**, *240*, 172−181.
(83) Groppo, E.; Estephane, J.; Lamberti, C.; Spoto, G.; Zecchina, A. *Catal. Today* **2007**, *126*, 228−234.
(84) Groppo, E.; Damin, A.; Otero Arean, C.; Zecchina, A. *Chem.—Eur. J.* **2011**, *17*, 11110−11114.
(85) Barzan, C.; Groppo, E.; Quadrelli, E. A.; Monteil, V.; Bordiga, S. *Phys. Chem. Chem. Phys.* **2012**, *14*, 2239−2245.

DOI: 10.1021/acscatal.5b01108
ACS Catal. 2015, 5, 5586−5595